Available online at www.sciencedirect.com
ScienceDirect
Trans. Nonferrous Met. Soc. China 34(2024) 1618−1633
Transactions of Nonferrous Metals Society of China
www.tnmsc.cn

Biocompatibility of Nb_2C MXene film for ophthalmic implants

Wei MA[1,2*], Li PENG[1,3*], Bai-hua CHEN[1,2]

1. Department of Ophthalmology, The Second Xiangya Hospital of Central South University, Changsha 410011, China;
2. Hunan Clinical Research Center of Ophthalmic Disease, Changsha 410011, China;
3. Department of Ophthalmology, Haikou Affiliated Hospital of Central South University Xiangya School of Medicine, Haikou 570311, China

Received 26 September 2023; accepted 23 April 2024

Abstract: The Nb_2C MXene film was prepared by tetrafluoroboric acid (HBF_4) and hydrofluoric acid (HF) etching and vacuum extraction. The surface structure, properties, and composition of Nb_2C MXene were characterized by scanning electron microscopy (SEM), atomic force microscopy (AFM), X-ray photoelectron spectroscopy (XPS), and other methods. The biocompatibility of Nb_2C MXene film was evaluated by in vivo and in vitro experiments. The results show the layered, micro−nano surface structure of Nb_2C MXene with abundant hydroxyl groups (—OH) on the surface. Compared with the control group, the proliferation rate of conjunctival fibroblasts cultured with 1 mg/mL Nb_2C MXene is 72.15% (p<0.05). The cytotoxicity of Nb_2C MXene is Grade 0 (p>0.05), and the hemolysis rate is 0.38% (<5%). The oxidative stress and inflammatory responses in rabbit ocular tissues are inhibited by Nb_2C MXene film, which promotes wound healing without inducing fibrosis, and its micro−nano structure promotes cell adhesion and proliferation, demonstrating good biocompatibility.

Key words: Nb_2C MXene; biocompatibility; oxidative stress; cell proliferation; ophthalmic application

1 Introduction

The demand for medical consumables is escalating due to the growing number of medical procedures. Hence, there is a need for new medical materials with excellent biocompatibility to be created [1−3]. Mechanical compatibility and biocompatibility with the human body are achieved by metal materials for medical purposes with excellent properties, such as fatigue resistance, mechanical strength, toughness and low cytotoxicity [4,5]. Furthermore, these materials are commonly utilized in the production of biological valves and other human implants because of their exceptional machinability [6,7].

MXenes, a novel class of two-dimensional early transition metal carbides, nitrides, and carbonitrides, have attracted significant attention since they were first reported in 2011 due to their remarkable characteristics, such as hydrophilicity, optical properties, and mechanical properties [8,9]. Two-dimensional niobium carbide (Nb_2C) is a novel type of MXene, which is found to exhibit an extremely high photothermal conversion efficiency in bone tumor ablation and to promote the proliferation, and differentiation of osteoblasts [10]. In recent years, increasing attention has been paid to Nb_2C MXene as a nanomedical material that can be utilized to create novel metal medical implants. There are a few studies on titanium−niobium alloys as orthopedic implants, niobium-based films as

*These authors contributed equally to this work
Corresponding author: Bai-hua CHEN, Tel: +86-13873158008, E-mail: chenbaihua2017@csu.edu.cn
DOI: 10.1016/S1003-6326(24)66495-2
1003-6326/© 2024 The Nonferrous Metals Society of China. Published by Elsevier Ltd & Science Press
This is an open access article under the CC BY-NC-ND license (http://creativecommons.org/licenses/by-nc-nd/4.0/)

dental implants, and niobium doping into metal alloys for dental implants. The advantages of niobium, such as antibiosis, corrosion resistance, low cytotoxicity, and wear resistance have been noticed [11−13]. Carbides have been discovered to enhance the electrical conductivity and resistance to carbon corrosion of gel networks, thus boosting the biocompatibility of the material [14−16]. Enhanced comprehension of the properties of Nb_2C MXenes resulting from the amalgamation of Nb and carbon will facilitate the identification of appropriate biomaterials. Nb_2C MXene has potential as a biological material in medical fields [17−19].

There are less reports on Nb_2C MXene-based materials in ophthalmology. Good biocompatibility, the ability to promote cell adhesion and proliferation, and a certain level of mechanical strength and toughness are required of the materials for artificial corneal scaffolds [20,21]. The ability to support the growth and repair of blood vessels, nerves, and surrounding soft tissues, as well as resistance to microbial adhesion, is required for ocular implants such as ocular prosthetics [22]. Excellent processability, surface modification capabilities, specific pro-angiogenic effects, and antibacterial properties have been observed in Nb_2C MXene [23], which can be combined with other materials or used as a surface coating to fabricate novel tissue engineering scaffolds. Various drugs and proteases can be adsorbed or covalently attached to Nb_2C MXene with a layered structure and high specific surface area, demonstrating the potential for drug loading and enzyme immobilization. This opens possibilities for developing novel Nb_2C MXene-based therapies and biosensing technologies.

This study aims to explore the biocompatibility and potential applications of Nb_2C MXene as a novel biomaterial in the field of ophthalmology and provide an experimental basis for the clinical application of Nb_2C MXene in ophthalmology.

2 Experimental

2.1 Material preparation and characterization

A mixture of HBF_4 and HF was heated to 40 °C in a conical flask, and Nb_2AlC powder was added to react with the solution. The reaction lasted for 52 h. Afterward, the multilayer Nb_2C powder was obtained by centrifuging and washing the mixture with ethanol until the pH was close to neutral and drying in a vacuum. Then, the Nb_2C powder was dispersed into tetrapropylammonium hydroxide (TPAOH) and stirred at room temperature for 3 d. Next, TPAOH was removed by centrifugation. The obtained solid was dispersed in distilled water and sonicated for 1 h. Finally, the aqueous dispersion of Nb_2C MXene nanosheets was collected by centrifuging the sonicated dispersion at 3000 r/min for 1 h. The Nb_2C nanosheets were stored in an aqueous suspension at 1 mg/mL. The Nb_2C MXene film was obtained by filtering 50 mL suspension of 5 mg/mL Nb_2C MXene suspension under a vacuum of 0.1 MPa at room temperature for 48 h and drying at room temperature.

The crystal structure of the Nb_2C MXene powder was identified by XRD (Rigaku DMAX2400). The microstructure of the Nb_2C MXene powder was observed by SEM (Hitachi SU8100), and the surface structure of the Nb_2C MXene film was observed by SEM and AFM (Bruker Dimension ICON). The elemental composition and chemical state of Nb_2C MXene were characterized by XPS (Thermo Scientific K-Alpha). The water contact angle of the Nb_2C MXene film was tested by a drop shape analyzer.

2.2 In vitro experiments

2.2.1 Hemolysis test of Nb_2C MXene

This test was carried out according to the method specified in YY/T 1651.1—2019 [24]. Healthy blood from New Zealand rabbits was mixed with 5 mL of sodium citrate (0.109 mol/L) in an anticoagulant blood collection vessel and diluted with normal saline at a volume ratio of 4:5. 1 mg and 10 mg of Nb_2C MXene were separately added to test tubes containing 10 mL of physiological saline. The tubes were preincubated at 37 °C for 30 min. Then, 0.2 mL of the diluted blood was added to each standard tube, and the mixtures were incubated at 37 °C for 60 min. Similarly, deionized water and standard saline solution were used as positive and negative controls. All the tubes were centrifuged at 3000 r/min for 5 min. Finally, the supernatants were withdrawn and transferred to new centrifuge tubes for spectroscopic analysis.

2.2.2 Cell proliferation and viability tests

Human orbital fibroblasts (Wuhan Primitive Biopharmaceutical Technology Company, HUM-

CELL-0336) and conjunctival fibroblasts (Wuhan Primitive Biopharmaceutical Technology Company, HUM-CELL-0337) were cultured in a humid environment containing 5% carbon dioxide (CO_2) at 37 °C in a specialized medium (DMEM/Ham's F12+5% FBS+5 μg/mL insulin+10 ng/mL human EGF+0.5% DMSO).

Cell proliferation was assessed by EdU assays (Beyotime Biotechnology, C0085L). The experiment consisted of control group, A group, and B group, with three wells per group. A group served as the low-concentration Nb_2C MXene intervention group, while B group served as the high-concentration Nb_2C MXene intervention group. Cells in the 3rd−5th generation were seeded on 24-well culture plates at a density of 30000 cells per well. Then, 0.1 mg Nb_2C MXene powder and 1 mL of cell-specific medium were added to A group, and 1 mg Nb_2C MXene powder and 1 mL cell-specific medium were added to B group. 1 mL of cell-specific medium was added to the control group. The cells in the control group, A group, and B group were cultured in a humid atmosphere at 37 °C with 5% CO_2 for 24 h. The subsequent steps were performed according to the company's EdU HTS kit protocol.

Cell viability was assessed by calcein AM assays (Beyotime Biotechnology, C2015M). The experimental grouping was the same as above. The subsequent steps were performed according to the Calcein AM kit protocol. The 24-well cell culture plate was observed under an optical microscope. Six areas were randomly selected to count cells.

The expression of Ki67, PCNA, and MCM2 in conjunctival fibroblasts (B group) was detected using real-time quantitative polymerase chain reaction (qPCR). The primers used for qPCR amplification are listed in Table 1. The experiment of all cells in each group was repeated three times.

2.3 In vivo experiments

2.3.1 Acute systemic toxicity tests

This test was conducted according to the method specified in GB/T 16886.11—2011 [25]. Two groups of mice were used for the acute toxicity test, and five mice were selected for each group. Sample extracts were prepared by soaking the Nb_2C MXene film in normal saline at 3 cm^2/mL at 37 °C for 72 h. The experimental group was intraperitoneally injected with the sample extracts, and the control group was injected with saline at a dose of 50 mL/kg. The mice were observed immediately and at 4, 24, 48, and 72 h after treatment. The survival rate, body weight, systemic inflammation, and animal behavior in each group were monitored as indexes of systemic reactions.

Table 1 Primers for qPCR amplifications

Primer	Oligo sequence of 5'-3'
Ki67(F)	AAGAAGCCCATGAAGACCTCC
Ki67(R)	CTCTTCTGCCCTCCGCTCT
PCNA(F)	TAGCTCCAGCGGTGTAAACCT
PCNA(R)	ACTTTCTCCTGGTTTGGTGCTT
MCM2(F)	TTGTTGCTGTAGTGGCGGA
MCM2(R)	GGAGGTGAGAGGATCATTGCC
actin(F)	ACCCTGAAGTACCCCATCGAG
actin(R)	AGCACAGCCTGGATAGCAAC

2.3.2 Implantation of Nb_2C MXene film in vivo

All the experimental procedures involving animals were approved by the Animal Ethics and Welfare Committee of the Second Xiangya Hospital of Central South University (No. 2022610). Eighteen adult male New Zealand white rabbits (mass 2.0−2.5 kg, age 3 months) were randomly divided into three sections, with each section containing three groups (n=2 per group). Nb_2C MXene films were cut into circular shapes with a diameter of 5 mm and subjected to ultraviolet disinfection. New Zealand white rabbits were anesthetized by intramuscular injection of ketamine and xylazine (0.6 mL/kg). One eye from each rabbit was randomly selected for surgery, and the contralateral eye served as a control in the nonsurgery or sham surgery groups. The groups were as follows.

Part one: The Nb_2C MXene film was placed in the conjunctival sac, and the incision was sutured with 10-0 sutures.

Part two: The Nb_2C MXene film was placed under the scleral flap, and the incision was sutured with 10-0 sutures.

Part three: The Nb_2C MXene film was placed under the skin incision around the orbital, and the skin incision was sutured with 5-0 sutures.

Slit lamp examinations were performed one day before surgery and 8 weeks after surgery to observe wound healing, inflammation, and rejection

reactions. The rabbits were euthanized 8 weeks post-surgery.

2.3.3 Analysis of oxidative stress indicators and inflammatory indicators

Each tissue collected from the area around the implant was crushed, homogenized, thoroughly mixed, and then centrifuged (3000 r/min, 4 °C) for 20 min. Then, the supernatant was separated. The expression level of malondialdehyde (MDA) was detected by the assay kit (Nanjing Jiancheng Bioengineering Institute, A003-1-1). The activities of SOD and GSH-Px were detected by the assay kits (Nanjing Jiancheng Bioengineering Institute, A001-3-1 and A005-1-2). The expression levels of IL-2 and IL-6 in each tissue were quantified by using rabbit IL-2 and IL-6 ELISA kits (Shanghai Huzhen Biotechnology Company, HZ-IL2-RAB, and HZ-IL6-RAB) according to the manufacturer's instructions.

2.3.4 Evaluation of inflammatory reactions and fibrosis by HE staining and immunohisto-chemical staining

Each tissue harvested from the area around the implants was fixed in 4% paraformaldehyde prior to histological analysis. Then, the prepared sections were dehydrated and embedded in paraffin wax, sectioned at a thickness of 4 μm, stained with hematoxylin and eosin (HE), and observed under a bright field microscope (Zeiss). A series of additional sections were subjected to immune-histochemistry, and the levels of cluster of differentiation 11b (CD11B) and alpha-smooth muscle actin (α-SMA) expression were used to evaluate inflammatory response and fibrotic proliferation.

2.4 Statistics

Data are presented as the means and standard deviation (SD). Differences among groups were compared using one-way ANOVA. The *R* statistical analysis package (version 3.5.3) was used to analyze the data statistically. An alpha value of $p<0.05$ was considered to indicate statistical significance in this study.

3 Results and discussion

3.1 Characterization

Figure 1(a) shows the Nb_2C MXene powder formed by etching with a mixture of HBF_4 and HF, which exhibits an accordion-like layered stacking structure. The XRD pattern shown in Fig. 1(b) reveals a shift in the characteristic peak of Nb_2C MXene to a lower 2θ position (from 12.8° to 4.8°), which suggests an increase in the interlayer spacing of MXene. The Nb_2C MXene was successfully synthesized, and Al was completely eroded and removed.

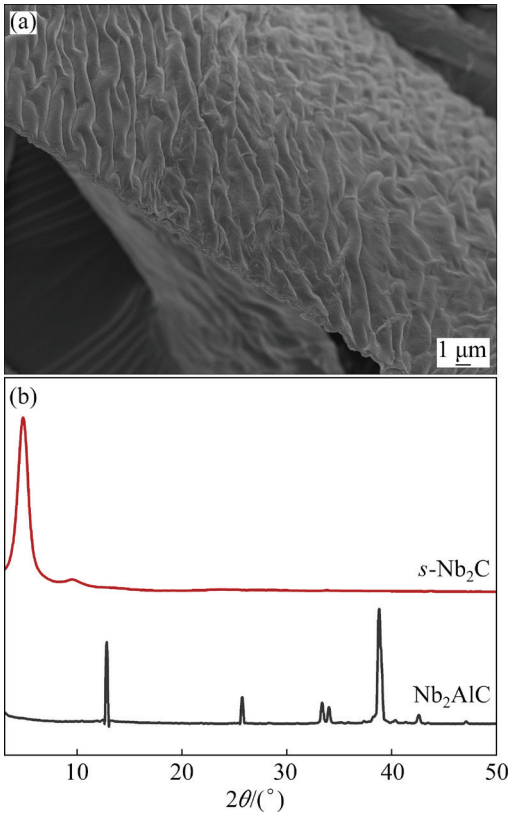

Fig. 1 Surface structure and phase composition of Nb_2C MXene powder: (a) SEM image of Nb_2C MXene powder; (b) XRD pattern of Nb_2C MXene powder

As shown in Fig. 2(b), the Nb_2C MXene film primarily consists of stacked Nb_2C MXene nano-sheets, demonstrating a porous structure within the film. Despite a wrinkled morphology, the surface of the Nb_2C MXene film remains relatively flat (Fig. 2(a)). Figure 2(c) presents a typical two-dimensional image of the surface morphology, revealing a nanoscale roughness of (79.8±2.2) nm for the Nb_2C MXene film surface. The surface properties of biomaterials, encompassing their chemical composition, electrical conductivity, roughness, stiffness, hydrophilicity/hydrophobicity, and micro−nano scale topographical structure, significantly influence cell proliferation and adhesion [26,27]. Cell adhesion is the process by

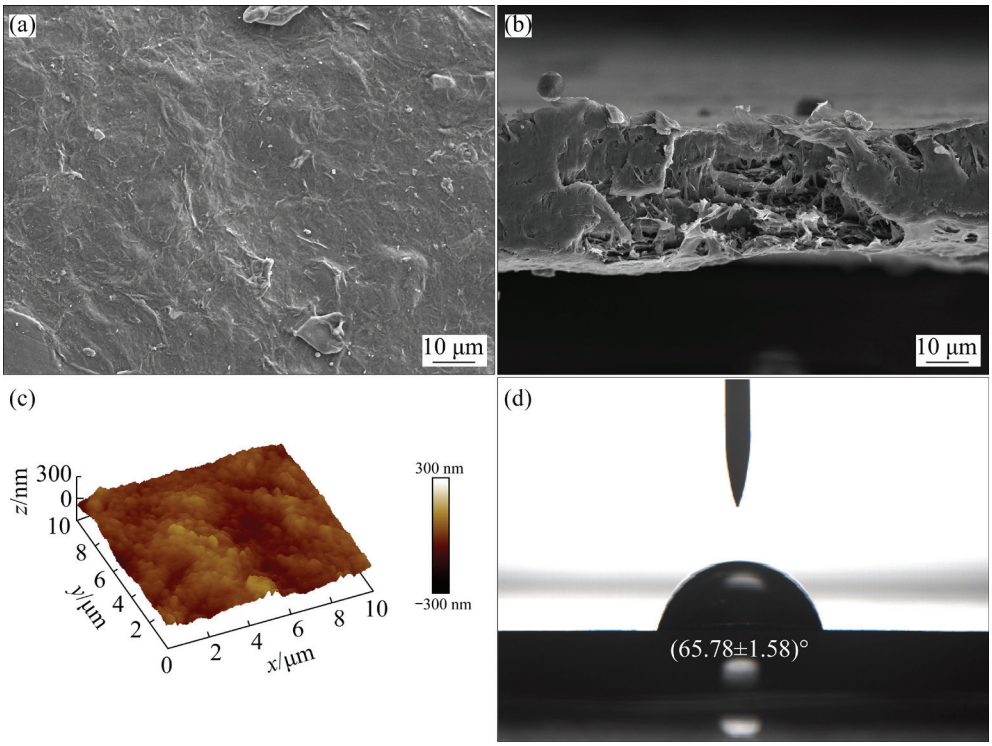

Fig. 2 Surface structure and properties of Nb_2C MXene flim: (a) SEM image of surface of Nb_2C MXene film; (b) SEM image of corss section of Nb_2C MXene film; (c) AFM image of Nb_2C MXene flim; (d) Water contact angle of Nb_2C MXene film

which cells interact with their surrounding environment, including other cells and the extracellular matrix. Better adhesion and proliferation of fibroblasts are observed on nano-island surfaces with heights of 10−100 nm [28]. The roughness of the Nb_2C MXene film surface affects cell and protein adhesion and proliferation. The anchoring and stability of proteins and the enhancement of protein adsorption are facilitated on the orderly grooved surface. The contact area between cells and the material is increased, and the orderliness of cellular distribution is improved by the high specific surface area of the material, which promotes cell adhesion and the formation of focal adhesion.

XPS analysis shown in Fig. 3(a) uncovers the overall composition of Nb_2C MXene film. The high-resolution O 1s XPS spectrum (Fig. 3(c)) shows three distinct peaks at 533.49 eV (—OH), 532.09 eV (C—Nb—O), and 530.44 eV (Nb—O). Terminal groups are formed on the layered MXene surface by the hydroxide ions in the strong acid etching solution, resulting in the generation of —OH. The —OH on the surface of Nb_2C MXene attracts water molecules through hydrogen bond interactions, enhancing the hydrophilicity of the material. Hydrophilic biomaterials enhance cell proliferation and adhesion [29]. Material surfaces with moderate hydrophilicity are more conducive to promoting cell adhesion and growth [30]. Figure 2(d) shows a typical image of a distilled water droplet on the sample surface, exhibiting a water contact angle of (65.78±1.58)°, indicative of the excellent hydrophilicity. The number of adsorption sites and the adsorption capacity on its surface are improved due to an increase in hydrophilicity, and growth factors and adhesion proteins are adsorbed from the extracellular matrix. The arrangement of the cellular skeleton is influenced by the aggregation of adhesive proteins, promoting cell proliferation.

3.2 Evaluation of biocompatibility

3.2.1 Blood compatibility

The hemolysis rate test results for Nb_2C MXene are presented in Table 2. According to the international standard ISO 10993-4, the hemolysis rate of medical materials should be less than 5%. The hemolysis rates (HR) of the 0.1 mg/mL and 1 mg/mL Nb_2C MXene are 0.38% and 0.52%, respectively,

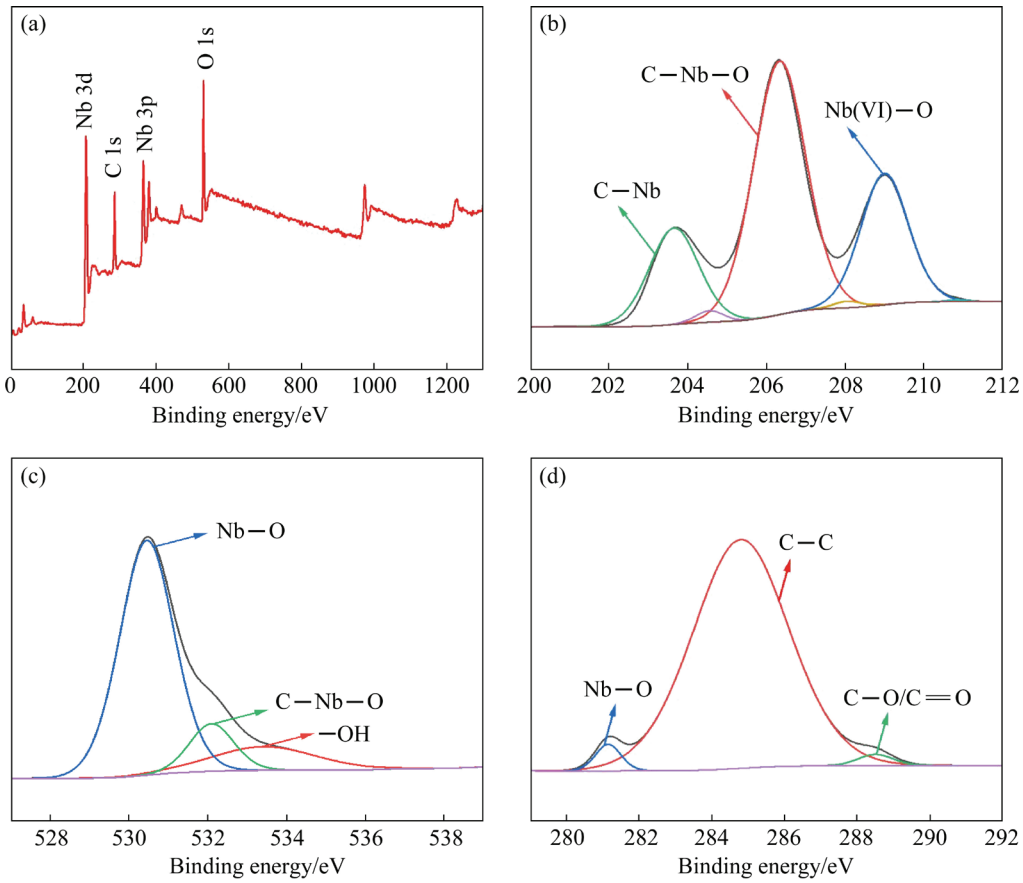

Fig. 3 XPS pattern of Nb_2C MXene flim: (a) Over view; (b) Nb 3d; (c) O 1s; (d) C 1s

Table 2 Hemolysis rate of Nb_2C Mxene

Group	OD	HR/%
0.1 mg/mL	0.0397±0.0001	0.38±0.0005
1 mg/mL	0.0408±0.00007	0.52±0.0003
Negative control	0.0376±0.0002	0
Positive control	0.6789±0.001	100

lower than 5% (p>0.05). The integrity of red blood cells is not compromised by the micro−nano structure of Nb_2C MXene. Compared to the hemolysis rates of other materials, such as Zn–3Sn alloy at 0.53% [31], titanium alloy at 1.1% [32], bioceramics such as graphene/titanium dioxide at 1.6% [33], and nanoporous structure of hydroxyapatite (HA) at 0.9% [34], Nb_2C MXene exhibits superior blood compatibility.

3.2.2 Cell viability and in vivo toxicity

In this work, live cells show green fluorescence, and the nuclei of dead cells show red fluorescence. No apparent death of human orbital fibroblasts or subconjunctival fibroblasts is observed in Fig. 4. The cells in A (Figs. 4(b, e)) and B (Figs. 4(c, f)) groups are evenly distributed, and almost no red fluorescence was visible. The relative survival rate (RSR) of cells in each group is shown in the histogram in Fig. 4. RSR for subconjunctival fibroblasts in A group and B group is reported as (107.2±3.3)% and (108.7±3.2)%, respectively, and for orbital fibroblasts, RSR is reported as (113.1±2.9)% and (121.1±1.8)% (p<0.05), indicating that Nb_2C MXene is nontoxic to these two types of cells. According to ISO 10993-5: 2009 [35], the cytotoxicity of Nb_2C MXene is evaluated as Grade 0. Strong interactions with cell membranes are not induced by Nb_2C MXene, and oxidative stress or inflammatory responses within cells are not triggered by it. The cytotoxicity of Ti_3C_2 MXene is significantly higher than that of Nb_2C MXene in the same concentration [36].

Figure 5 shows the changes in mice's body mass and behavioral performance at 4, 24, 48, and 72 h after intraperitoneal injection of sample extracts. There is no significant difference in the changes in body mass of the mice in the experimental group and the control group (p>0.05).

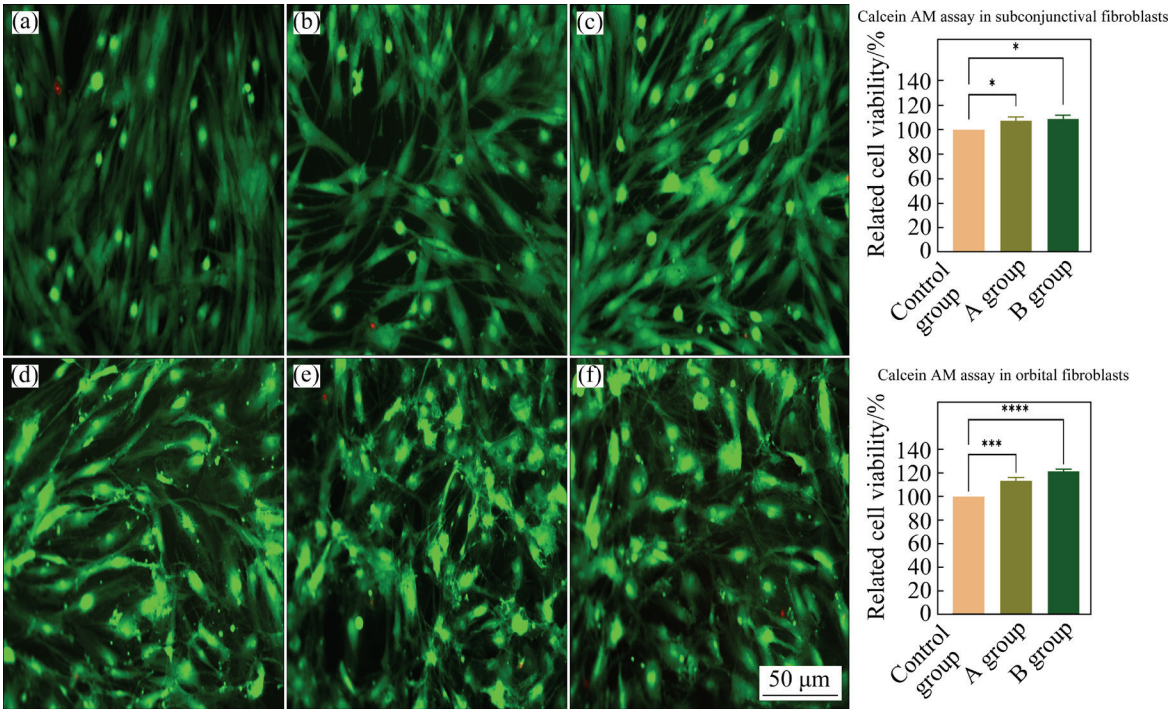

Fig. 4 Effects of Nb_2C MXene on cell viability: Cell viability of orbital fibroblasts (a) and subconjunctival fibroblasts (d) in control group; Cell viability of orbital fibroblasts (b) and subconjunctival fibroblasts (e) in A group; Cell viability of orbital fibroblasts (c) and subconjunctival fibroblasts (f) in B group

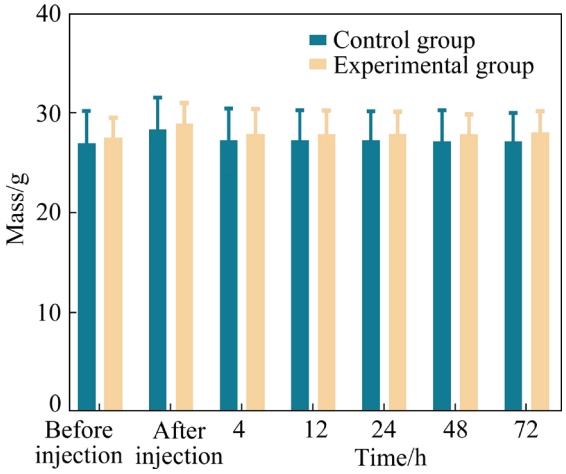

Fig. 5 Mass changes of mice after intraperitoneal injection of sample extracts

No abnormal behaviors or systemic inflammatory reactions, such as weakness, cyanosis, or dyspnea, are found in the mice during the experiment, which indicates that Nb_2C MXene has no systemic toxicity in mice.

3.2.3 Cell proliferation

Figure 6 shows the results of cell proliferation. Proliferating cells show green fluorescence, and the cell nuclei show blue fluorescence. The highest proportion of proliferating cells in B group is shown in Figs. 6(c, f), followed by A group (Figs. 6(b, e)), while the lowest proportion of proliferating cells in the control groups is shown in Figs. 6(a, d). The histogram on the rightmost side of Fig. 6 shows the proportion of proliferating cells in the three groups. The average variable proliferation index in A and B groups is significantly higher than that in the control groups (p<0.05). For orbital fibroblasts, the cell proliferation rate is (68.51±0.77)% for 0.1 mg/mL Nb_2C MXene co-culture, (71.48±1.25)% for 1 mg/mL Nb_2C MXene co-culture, and (63.63±1.00)% for the control group. For subconjunctival fibroblasts, the cell proliferation rate is (66.47±0.99)% for 0.1 mg/mL Nb_2C MXene co-culture, (72.15±1.57)% for 1 mg/mL Nb_2C MXene co-culture, and (62.26±1.27)% for the control group. Cell proliferation is significantly promoted by both concentrations of Nb_2C MXene, with the best effect being observed at 1 mg/mL Nb_2C MXene. The aggregation of growth factors and adhesion proteins is potentially caused by the vigorous adsorption of Nb_2C MXene, impacting integrin signaling on the cell membrane, leading to activation of the PI3K/Akt-mTOR signaling pathway, and promoting cell proliferation. Other research indicates that cell growth and metabolism

can be promoted by Nb_2C MXene through the conduction of microcurrent stimulation [37].

The expression levels of the proliferation-related genes Ki67, PCNA, and MCM2 in the three groups of subconjunctival fibroblasts were measured. Figures 7(a−c) show that the expression levels of these genes in A and B groups are higher than those in the control group (p<0.05). A high expression of these proteins is observed in mitotic cells [38−40]. The expression levels of PCNA and MCM2 in the B group are higher than those in A group. However, the expression levels of Ki67 do not correlate entirely positively with the concentration of Nb_2C MXene. The expression levels of Ki67 in the A group is lower than that in B group but higher than that in the control group. Ultrahigh concentrations of Nb_2C MXene may exert some inhibitory effect on cell proliferation.

Figure 8 shows SEM morphology of the surface of the Nb_2C MXene film implanted under the conjunctiva for three months. The cells are flat and spindle-like, with a good growth state, which adhere firmly to the surface of the film and connect to each other through filopodia and extracellular protrusions.

3.2.4 Clinical reactions

Figure 9 shows the clinical observation results of implanting Nb_2C MXene film into rabbit eyes for

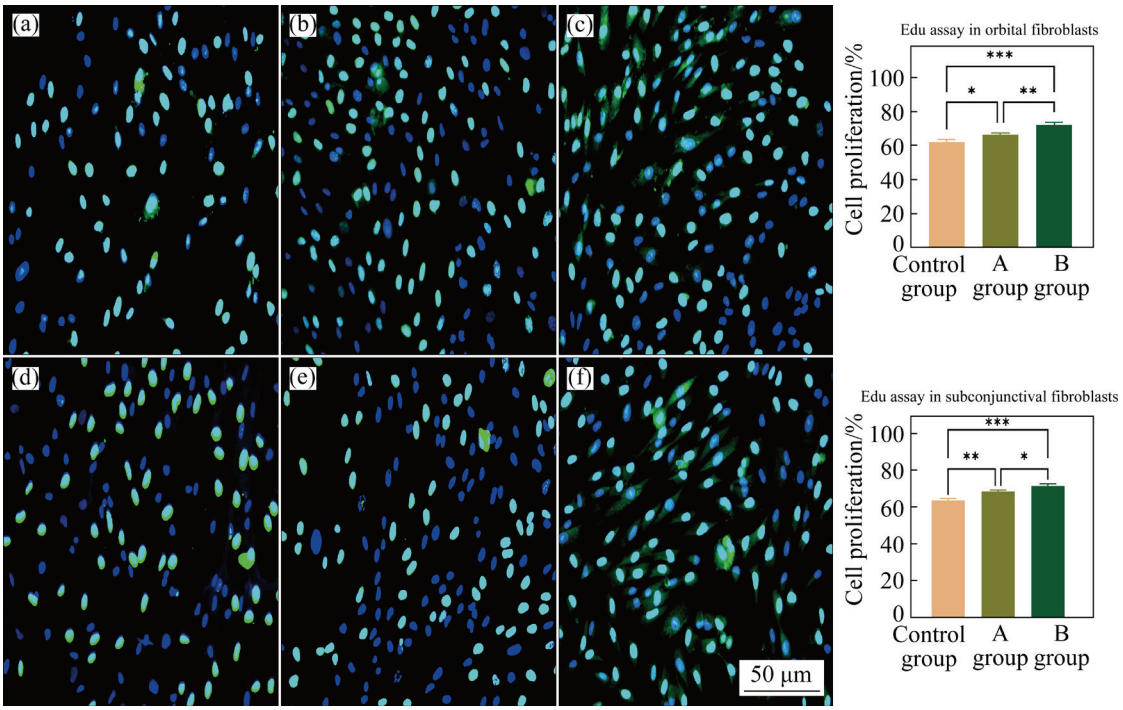

Fig. 6 Effect of Nb_2C MXene on cell proliferation: Cell proliferation index of orbital fibroblasts (a) and subconjunctival fibroblasts (d) in control group; Cell proliferation index of orbital fibroblasts (b) and subconjunctival fibroblasts (e) in A group; Cell proliferation index of orbital fibroblasts (c) and subconjunctival fibroblasts (f) in B group

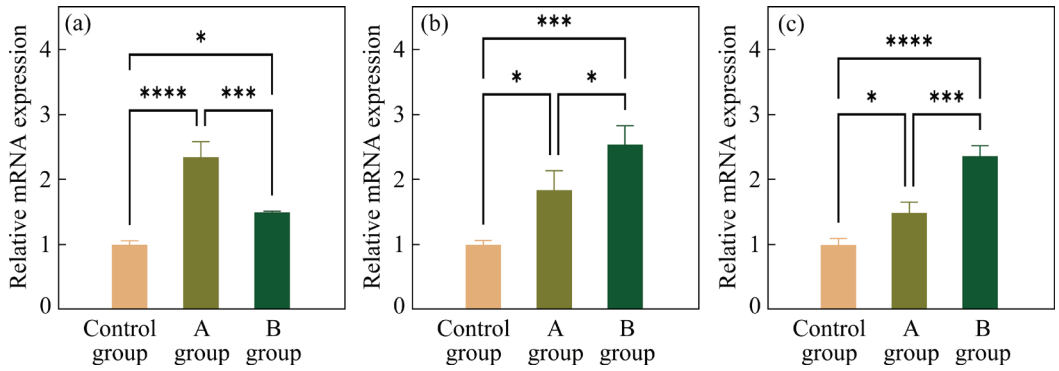

Fig. 7 Effect of Nb_2C MXene on cell proliferation gene: (a) Expression of Ki67 in different groups; (b) Expression of MCM2 in different groups; (c) Expression of PCNA in different groups

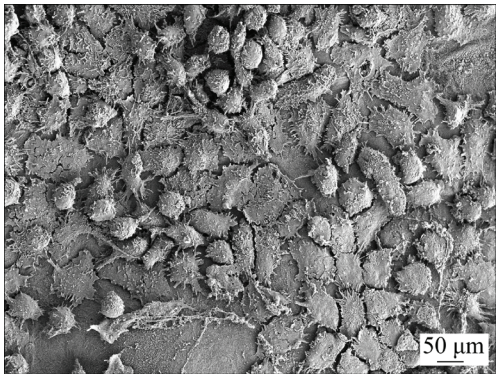

Fig. 8 SEM image of surface of Nb_2C MXene film after implantation

one day and eight weeks. At one day after the surgery, hemorrhage and erythema are observed in the surgical area of both the experimental groups (Figs. 9(a_3, c_3, e_3)) and sham groups (Figs. 9(a_2, c_2, e_2)). There are no discernible differences between the two groups. At the eighth week after the surgery, the hemorrhage disappears in the surgical area of the experimental groups. There are no signs of hyperemia, erythema, or neovascularization, indicating a favorable healing process and minimal postoperative scars (Figs. 9(b_3, d_3, f_3)). The performance is indistinguishable from that of the control groups (Figs. 9(b_1, d_1, f_1)). Although the hemorrhage also disappears in the sham group without the film, neovascularization indicates a postoperative inflammatory response (Fig. 9(d_2)), which shows that the inflammatory response is even inhibited by the Nb_2C MXene film.

Any apparent local inflammation, infection, or tissue scarring is not caused when the Nb_2C MXene film is implanted into rabbit eyes. No behavioral abnormalities, including loss of appetite, mass loss, discomfort, depression, stress, or physical disability, are observed in the test. All of the rabbits survive until the end of the experiment.

3.2.5 Oxidative stress

Figure 10 shows the expression levels of MDA and the activities of SOD and GSH-Px in three groups, which evaluate the effects of Nb_2C MXene on oxidative stress. Compared to the control group and the sham group, the levels of MDA in the conjunctiva, sclera, and subcutis are significantly reduced in the experimental groups (Figs. 10(d−f)). MDA is the final product of reactive oxygen species lipid peroxidation and a sign of peroxide damage [41]. The inhibition of tissue oxidative stress by the Nb_2C MXene film is suggested by the low levels of MDA in the experimental groups. The activity of SOD and GSH-Px increases dramatically in the experimental groups (p<0.05; Figs. 10(a−c, g−i)). SOD is an antioxidant enzyme that catalyzes superoxide into hydrogen peroxide, scavenges

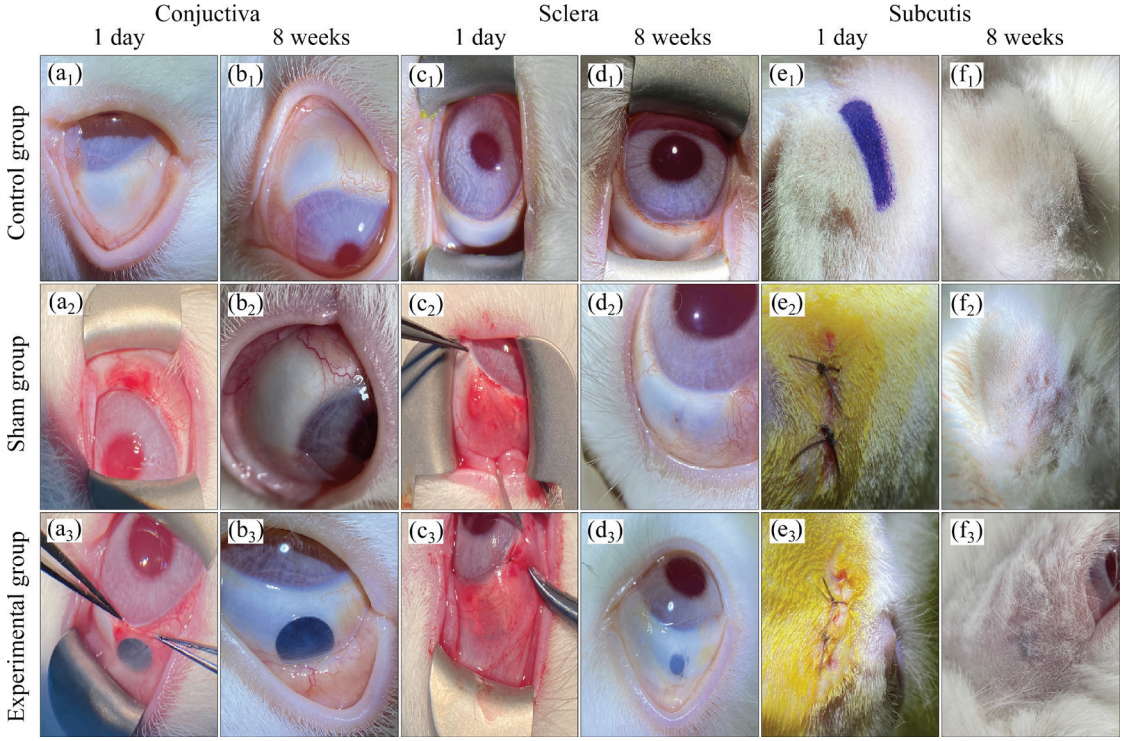

Fig. 9 Postoperative clinical photographs after 1 day and 8 weeks of post-surgery of rabbits

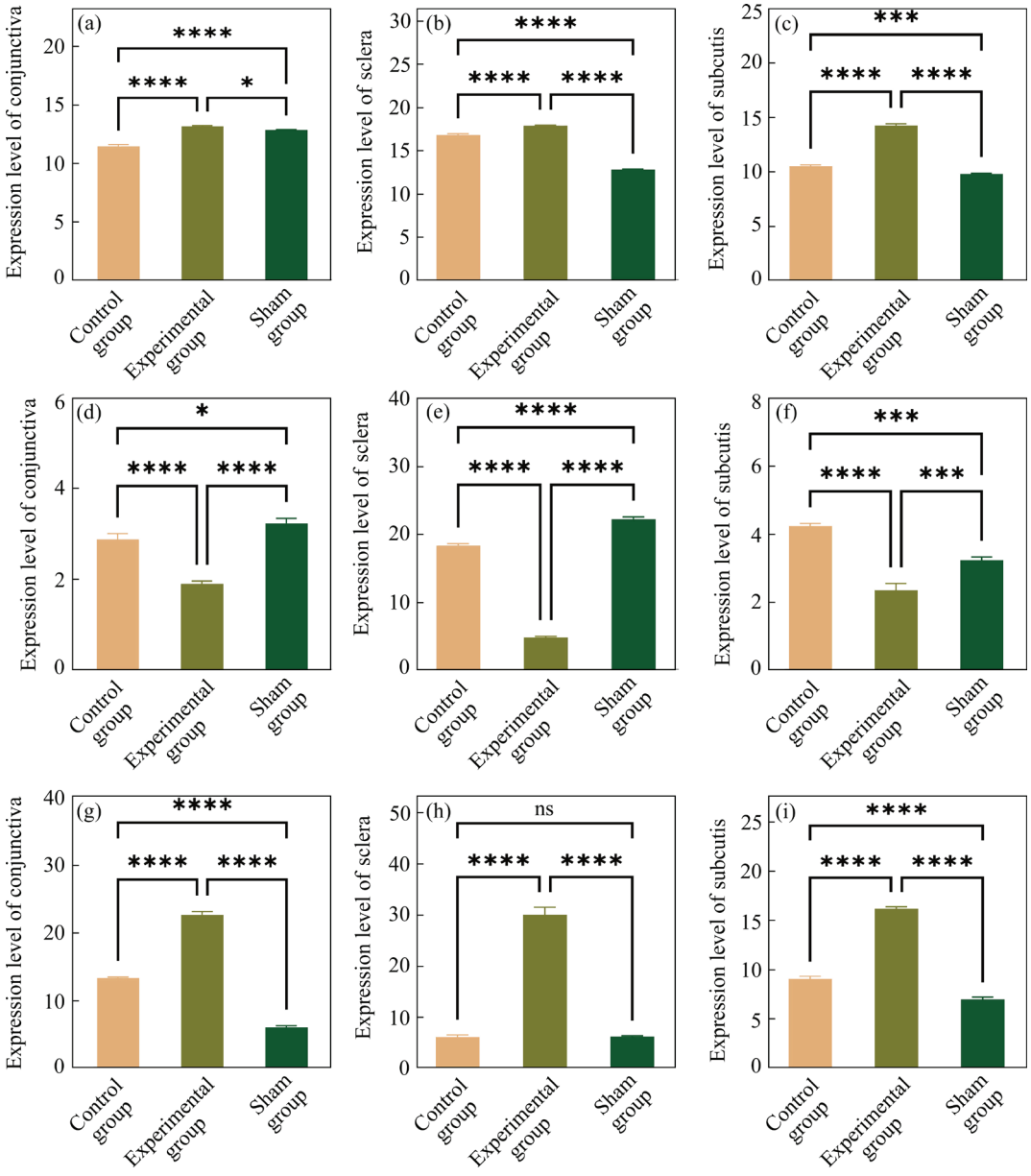

Fig. 10 Results of indicators related to oxidative stress expression levels: (a−c) SOD level of conjunctiva, sclera, and subcutis in three groups; (d−f) MDA level of conjunctiva, sclera, and subcutis in three groups; (g−i) GSH-Px level of conjunctiva, sclera, and subcutis in three groups

superoxide anions, and removes superoxide anion free radicals to protect cells from damage [42,43]. GSH-Px is an enzyme that decomposes H_2O_2. It blocks oxidative reactions related to functionality, reflecting antioxidant defense capabilities [44,45]. The depletion and inactivation of SOD and GSH-Px could potentially be caused by excessive oxidative stress. An enhancement of these two enzymatic activity is facilitated by the scavenging of reactive oxygen species (ROS) by Nb_2C MXene film.

Oxidative stress refers to the imbalance between ROS within cells and the antioxidant system, damaging cells and tissues. Oxidative stress is related to various diseases, such as cancer, cardiovascular diseases, and diabetes [46]. Reducing oxidative stress is a new area of focus in biomaterial research, influencing the fields of tissue engineering and regenerative medicine. Biomaterials alleviate or prevent damage to cells and tissues caused by oxidative stress through their antioxidant functions, thereby enhancing the biocompatibility and efficacy of the biomaterials [47]. Hydroxyl complexes are formed stably by the adsorption of OH^- at the [Nb3C] sites

on the surface of Nb_2C MXene. The O^{2-} is captured effectively by the oxygen vacancies present on the surface of the Nb_2C MXene, leading to the formation of superoxide complexes. In addition, Nb_2C MXene demonstrates the ability to catalyze the conversion of hydrogen peroxide into water and oxygen. The oxidative stress response can be effectively inhibited by Nb_2C MXene due to its reductive and catalytic properties.

3.2.6 Inflammation and tissue fibrosis

Figures 11−13 show the results of changes in the tissue inflammatory response. Determination of the inflammatory reaction index is an essential part of biocompatibility evaluation [48]. The less inflammation caused by the material is, the higher the biocompatibility is [49]. There are no histological differences observed in the conjunctiva, sclera, and subcutis of rabbits 8 weeks after implantation. No tissue involvement or damage is observed in the implantation area (Figs. 11(g−i)).

The immunofluorescence shows that the inflammatory marker CD11B is not detected in the experimental groups (Figs. 12(g−i)), and CD11B is rarely expressed in the conjunctival epithelium of the sham group (Fig. 12(d)) and the control group (Fig. 12(a)). CD11B is the α chain of the integrin CD11B/CD18 (alphaMbeta2, CR3, and Mac-1), which is usually expressed on the surface of infiltrating macrophages and neutrophils. The cell adhesion, migration, phagocytosis, and inflammation promotion are regulated by CD11B [50]. Their results suggest that inflammation and immunoreaction are not caused by the implantation of the Nb_2C MXene film. Moreover, compared to the control group and the sham group, the expression levels of the proinflammatory factors IL-2 and IL-6 are significantly reduced in the experimental groups (Figs. 13(a−f)). IL-2 and IL-6 are essential pro-inflammatory factors [51,52], and IL-6 plays vital roles in angiogenesis and inflammatory reactions in various eye parts [53]. In inflammatory responses, an increase in intracellular levels of ROS stimulates the production and release of IL-6 either directly or indirectly. The vicious cycle between oxidative stress and IL-6-mediated inflammation can be interrupted by clearing excess ROS, alleviating the inflammatory response. Simultaneously, inhibition of ROS-related MAPK/ERK and NF-kappaB signal transduction suppresses the expression of M1-type macrophages,

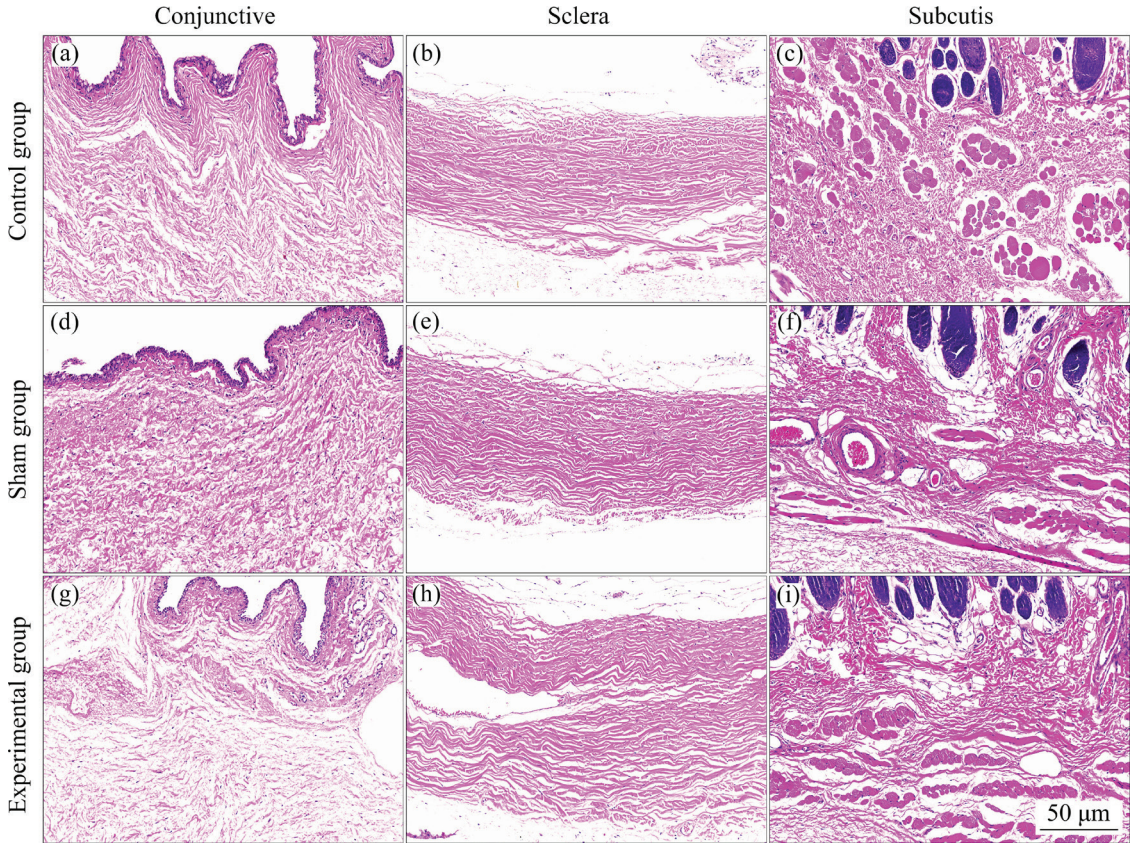

Fig. 11 Results of HE staining in three groups

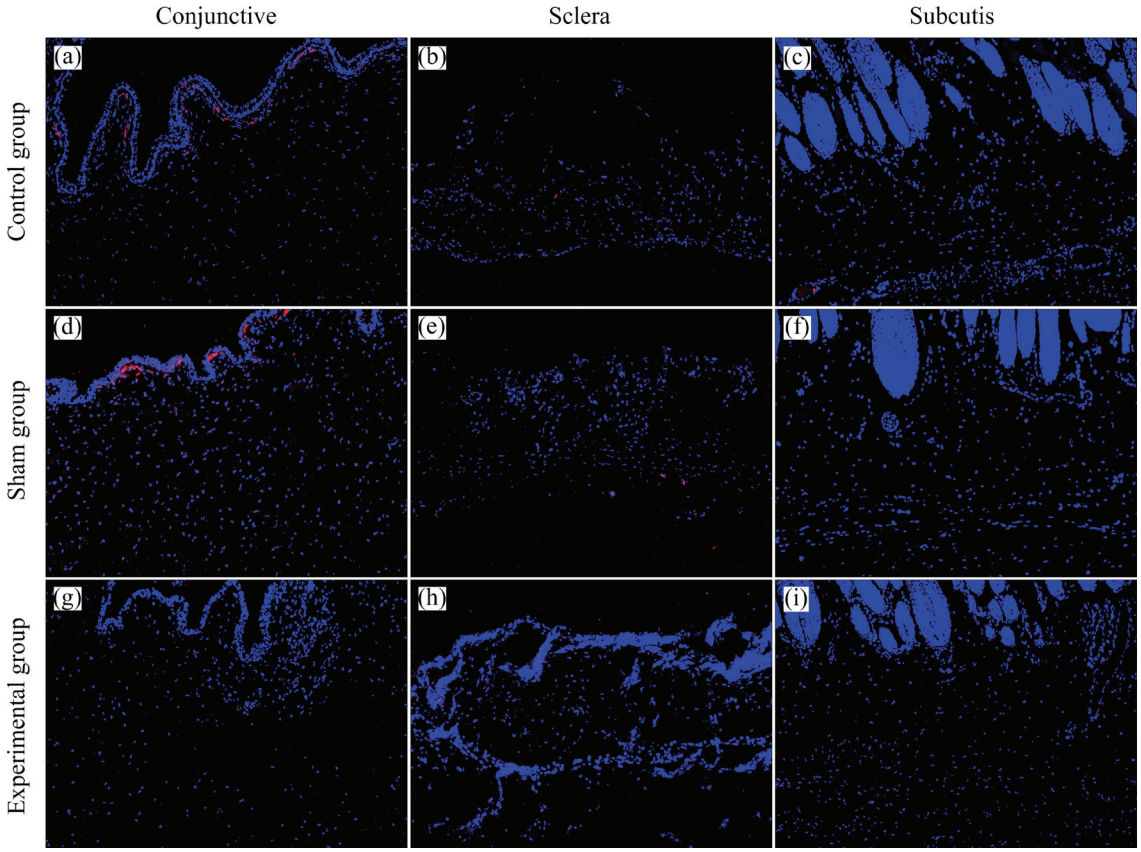

Fig. 12 Results of CD11B expression in three groups

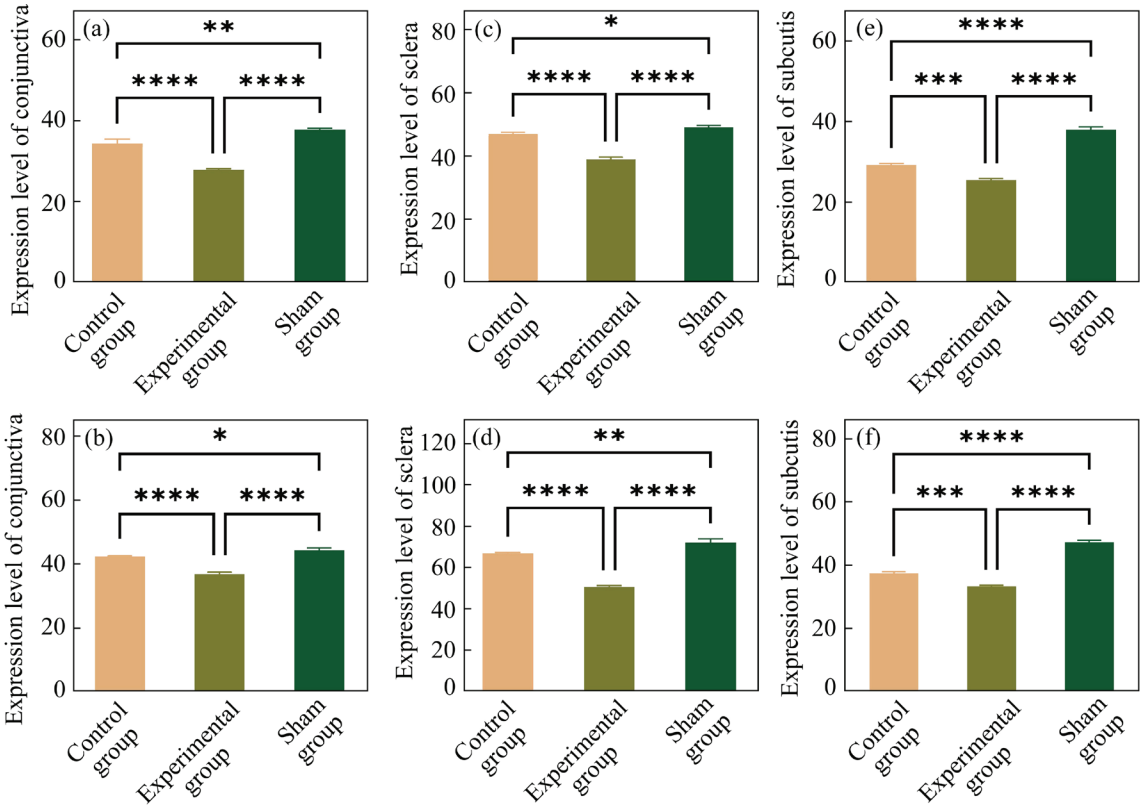

Fig. 13 Results of inflammatory cytokines level in three groups: (a, c, e) IL-2 level; (b, d, f) IL-6 level

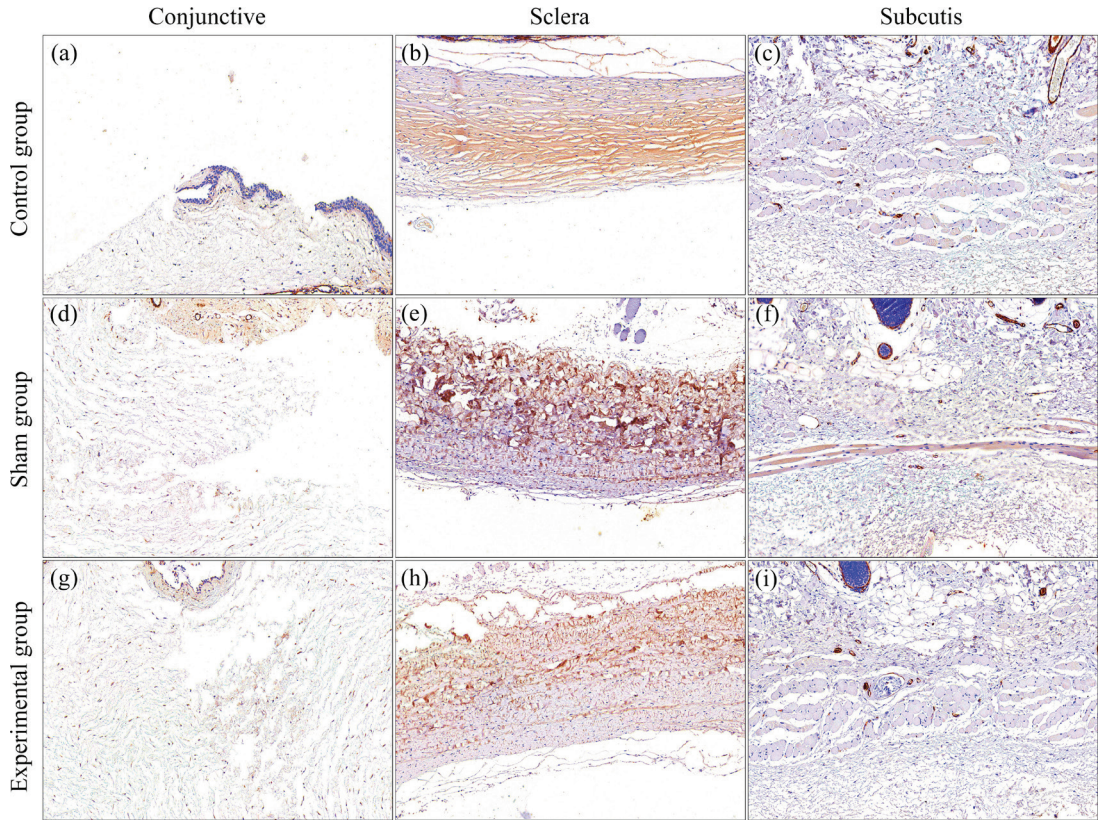

Fig. 14 Results of α-SMA expression in three groups

reducing the levels of pro-inflammatory factors [54,55]. The polarization of macrophages towards the M2 type is regulated by low levels of ROS through the STAT6 and PPARγ pathways, releasing anti-inflammatory and growth factors [56]. Nb_2C MXene film inhibits inflammation.

Figure 14 shows the immunohistochemical results for the expression of α-SMA. α-SMA is recognized as a marker of myofibroblasts, with positive staining appearing brownish-yellow. Compared to the sham groups (Figs. 14(d, e)), the positive signal for α-SMA in the conjunctiva and sclera of the experimental groups is weaker (Figs. 14(g, h)). The positive signal in the subcutis of the experimental group is similar to that of the control groups (Figs. 14(c, i)) and much weaker than that of the sham group (Fig. 14(f)). Wound fibrosis involves the activation of immune and inflammatory responses. The abnormal proliferation and activation of fibroblasts are stimulated by these responses, leading to excessive deposition of collagen in the connective tissue [57,58]. The fibrotic occurrence is prevented by the excellent immunological inertness and inhibition of the inflammatory response of Nb_2C MXene film.

4 Conclusions

(1) The Nb_2C MXene film was prepared by a mixture of HBF_4 and HF etching and vacuum filtration, which shows good hydrophilicity and micro−nano structures (R_a=(79.8±2.2) nm), promoting adhesion and proliferation of cells.

(2) No significant cytotoxicity is exhibited by Nb_2C MXene, and it is evaluated as Grade 0 for cytotoxicity. Good hemocompatibility is demonstrated by Nb_2C MXene, with a hemolysis rate of only 0.39%.

(3) Excellent implantation effects of Nb_2C mxene film are observed in rabbit eyes. The film is closely integrated with the ocular tissues and promotes wound healing. No adverse reactions or fibrosis are induced by the implantation of the Nb_2C MXene film. Oxidative stress and inflammatory responses in tissues are inhibited by the Nb_2C MXene film. The Nb_2C mxene film shows excellent biocompatibility.

CRediT authorship contribution statement

Wei MA: Methodology, Validation, Formal analysis,

Writing − Original draft; **Li PENG:** Methodology, Investigation, Formal analysis; **Bai-hua CHEN:** Methodology, Conceptualization, Writing − Review & Editing, Supervision, Project administration, Funding acquisition.

Declaration of competing interest

The authors declare that they have no known competing financial interests or personal relationships that could have appeared to influence the work reported in this paper.

Acknowledgments

This work was supported by the National Natural Science Foundation of China (Nos. 82171030, 81870678), Natural Science Foundation of Hunan Province, China (No. 2021JJ30925), Health Commission of Hunan Province, China (No. B202307026146) and Natural Science Foundation of Hainan Province, China (No. 821QN1005).

References

[1] LIU Tong-zhu, SHEN Ai-zong, HU Xiao-jian, TONG Gui-xian, GU Wei, YANG Shan-lin. SPD-based logistics management model of medical consumables in hospitals [J]. Iranian Journal of Public Health, 2016, 45(10): 1288−1299.

[2] ZHANG Lei, YANG Guo-jing, JOHNSON B N, JIA Xiao-feng. Three-dimensional (3D) printed scaffold and material selection for bone repair [J]. Acta Biomaterialia, 2019, 84: 16−33.

[3] HU Jing-jie, ALBADAWI H, CHONG B W, DEIPOLYI A R, SHETH R A, KHADEMHOSSEINI A, OKLU R. Advances in biomaterials and technologies for vascular embolization [J]. Advanced Materials, 2019, 31(33): e1901071.

[4] FERNANDES K R, ZHANG Yang, MAGRI A M P, RENNO A C M, BEUCKEN J J J P V D. Biomaterial property effects on platelets and macrophages: An in vitro study [J]. ACS Biomaterials Science & Engineering, 2017, 3(12): 3318−3327.

[5] CHON J W, YANG Xin, LEE S M, KIM Y J, JEON I S, JHO J Y, CHUNG D J. Novel peek copolymer synthesis and biosafety−I: Cytotoxicity evaluation for clinical application [J]. Polymers (Basel), 2019, 11(11): 1803.

[6] PHAM D H, ROO B D, NGUYEN X B, VERVAELE M, KECSKÉS A, NY A, COPMANS D, VRIENS H, LOCQUET J P, HOET P, WITTE P A M D. Use of zebrafish larvae as a multi-endpoint platform to characterize the toxicity profile of silica nanoparticles [J]. Scientific Reports, 2016, 6: 37145.

[7] DHANALAKSHMI A, PALANIMURUGAN A, NATARAJAN B. Enhanced antibacterial effect using carbohydrates biotemplate of ZnO nano thin films [J]. Carbohydr Polym, 2017, 168: 191−200.

[8] AL-ANTAKI A H M, KELLICI S, POWER N P, LAWRANCE W D, RASTON C L. Continuous flow vortex fluidic-mediated exfoliation and fragmentation of two-dimensional MXene [J]. Royal Society Open Science, 2020, 7(5): 192255.

[9] SIMON P. Two-dimensional MXene with controlled interlayer spacing for electrochemical energy storage [J]. ACS Nano, 2017, 11(3): 2393−2396.

[10] YIN Jun-hui, PAN Shan-shan, GUO Xiang, GAO You-shui, ZHU Dao-yu, YANG Qian-hao, GAO Jun-jie, ZHANG Chang-qing, CHEN Yu. Nb_2C MXene-functionalized scaffolds enables osteosarcoma phototherapy and angiogenesis/osteogenesis of bone defects [J]. Nano Letters, 2021, 13(1): 30.

[11] XU Jian, WENG Xiao-jun, WANG Xu, HUANG Jia-zhang, ZHANG Chao, MUHAMMAD H, MA Xin, LIAO Qian-de. Potential use of porous titanium-niobium alloy in orthopedic implants: Preparation and experimental study of its biocompatibility in vitro [J]. PLoS One, 2013, 8(11): e79289.

[12] ZHANG Xiang-yu, LU Shu-xin, HE Dong-mei, CHAI Mao-zhou, WU Zhuang-zhuang, YAO Xiao-hong, YANG Yong-qiang. Antibacterial property of graphene quantum dots-modified TiO_2 nanorods on titanium dental implant [J]. Transactions of Nonferrous Metals Society of China, 2023, 33(8): 2395−2405.

[13] SOUZA L P L D, LOPES J H, FERREIRA F V, MARTIN R A, BERTRAN C A, CAMILLI J A. Evaluation of effectiveness of 45S5 bioglass doped with niobium for repairing critical-sized bone defect in vitro and in vivo models [J]. Journal of Biomedical Materials Research: Part A, 2020, 108(3): 446−457.

[14] KANG Yu-qiong, DENG Chang-jian, CHEN Yu-qing, LIU Xin-yi, LIANG Zheng, LI Tao, HU Quan, ZHAO Yun. Binder-free electrodes and their application for Li-ion batteries [J]. Nanoscale Research Letters, 2020, 15(1): 112.

[15] DAI Hong-lian, WANG Xin-yu, HUANG Jian, YAN Yu-hua, LI Shi-pu. Effect of carbon fiber on calcium phosphate bone cement [J]. Transactions of Nonferrous Metals Society of China, 2004, 14(4): 769−774.

[16] LEI Ze-yuan, LIU Ting, LI Wei-juan, SHI Xiao-hua, FAN Dong-li. Biofunctionalization of silicone rubber with microgroove-patterned surface and carbon-ion implantation to enhance biocompatibility and reduce capsule formation [J]. International Journal of Nanomedicine, 2016, 11: 5563−5572.

[17] YATE L, COY L E, GREGUREC D, APERADOR A, MOYA S E, WANG Guo-cheng. Nb−C nanocomposite films with enhanced biocompatibility and mechanical properties for hard-tissue implant applications [J]. ACS Applied Materials & Interfaces, 2015, 7(11): 6351−6358.

[18] KANYO N, KOVACS K D, SAFTICS A, SZEKACS I, PETER B, SANTA-MARIA A R, WALTER F R, DÉR A, DELI M A, HORVATH R. Glycocalyx regulates the strength and kinetics of cancer cell adhesion revealed by biophysical models based on high resolution label-free optical data [J]. Scientific Reports, 2020, 10(1): 22422.

[19] XU Zheng-jiang, YATE L, QIU Yuan, APERADOR W, MOYA S E, WANG Guo-cheng. Potential of niobium-based thin films as a protective and osteogenic coating for dental

implants: The role of the nonmetal elements [J]. Materials Science and Engineering C, 2019, 96: 166−175.

[20] FANG Yin-dong, XIAO Ma, FEI Huang-yi. Implantation of hydroxyapatite-titanium corneal implants in rat cornea [J]. Cornea, 2011, 30(1): 67−72.

[21] LONG Yu-yu, ZHAO Xuan, LIU Sa, CHEN Min, LIU Bing-qian, JIAN Ge, JIA Yong-guang, REN Li. Collagen-hydroxypropyl methylcellulose membranes for corneal regeneration [J]. ACS Omega, 2018, 3(1): 1269−1275.

[22] XU Pei-fang, CAO Jing, FENG Xue, GAO Qi, LEE S Y, YE J. Facile fabrication of elastic, macroporous, and fast vascularized silicone orbital implant [J]. Journal of Biomedical Materials Research: Part B−Applied Biomaterials, 2021, 109(5): 765−774.

[23] YANG Chuang, LUO Yao, LIN Han, GE Min, SHI Jian-lin, ZHANG Xian-long. Niobium carbide MXene augmented medical implant elicits bacterial infection elimination and tissue regeneration [J]. ACS Nano, 2021, 15(1): 1086−1099.

[24] YY/T 1651.1 — 2019. Tests for hemolysis of medical devices-part 1: Material induced hemolysis assay [S].

[25] GB/T 16886.11—2011. Biological evaluation of medical devices-part 11: Test for systemic toxicity [S].

[26] KUMAR S, PAREKH S H. Linking graphene-based material physicochemical properties with molecular adsorption, structure and cell fate [J]. Communications Chemistry, 2020, 3(1): 8.

[27] CUI Di, KONG Na, DING Liang, GUO Ya-chong, YANG Wen-rong, YAN Fu-hua. Ultrathin 2D titanium carbide MXene (Ti_3C_2TX) nanoflakes activate WNT/HIF-1α-mediated metabolism reprogramming for periodontal regeneration [J]. Advanced Healthcare Materials, 2021, 10(22): e2101215.

[28] YANG Yong, WANG Kai, GU Xiao-song, LEONG K W. Biophysical regulation of cell behavior-cross talk between substrate stiffness and nanotopography [J]. Engineering (Beijing), 2017, 3(1): 36−54.

[29] ZHANG Yi-neng, YANG Hai-lin, JUAIM A N, CHEN Xiao-na, LU Chang, ZOU Ling, WANG Yin-zhou, ZHOU Xiong-wen. Biocompatibility and osteogenic activity of Zr−30Ta and Zr−25Ta−5Ti sintered alloys for dental and orthopedic implants [J]. Transactions of Nonferrous Metals Society of China, 2023, 33(3): 851−864.

[30] HAO Li-jing, YANG Hui, DU Chang, FU Xiao-ling, ZHAO Na-ru, XU Su-ju, CUI Fu-zhai, MAO Chuan-bin, WANG Ying-jun. Directing the fate of human and mouse mesenchymal stem cells by hydroxyl-methyl mixed self-assembled monolayers with varying wettability [J]. Journal of Materials Chemistry B, 2014, 2(30): 4794−4801.

[31] YAN Ting-liang, WANG Xiang, FAN Jin-long, NIE Qi-dong. Microstructure and properties of biodegradable co-continuous (HA+β-TCP)/Zn−3Sn composite fabricated by vacuum casting−infiltration technique [J]. Transactions of Nonferrous Metals Society of China, 2023, 31(10): 3075−3086.

[32] MANIVASAGAM V K, POPAT K C. In vitro investigation of hemocompatibility of hydrothermally treated titanium and titanium alloy surfaces [J]. ACS Omega, 2020, 5(14): 8108−8120.

[33] WU Xun-hui, LIEW Y K, LIM W M, MAI Chun-wai. Blood compatible and noncytotoxic superhydrophobic graphene/titanium dioxide coating with antibacterial and antibiofilm properties [J]. Journal of Applied Polymer Science, 2023, 140(11): e53629.

[34] OOI C H, LING Y P, ABDULLAH W Z, MUSTAFA A Z. Physicochemical evaluation and in vitro hemocompatibility study on nanoporous hydroxyapatite [J]. Journal of Materials Science−Materials in Medicine, 2019, 30(4): 44.

[35] ISO 10993-5: 2009. Biological evaluation of medical devices-part 5: Tests for in vitro cytotoxicity [S].

[36] GU Man-yu, DAI Zhi-qi, YAN Xiang, MA Jun-fei, NIU Ying-chun, LAN Wen-jie, WANG Xin, XU Quan. Comparison of toxicity of Ti_3C_2 and Nb_2C Mxene quantum dots (QDS) to human umbilical vein endothelial cells [J]. Journal of Applied Toxicology, 2021, 41: 745−754.

[37] ZHANG Zhong, GAO Shan, HU Yang-nan, CHEN Xin, CHENG Cheng, FU Xiao-long, ZHANG Sha-sha, WANG Xin-lin, CHE Yu-wei, ZHANG Chen, CHAI Ren-jie. $Ti_3C_2T_x$ MXene composite 3D hydrogel potentiates mtor signaling to promote the generation of functional hair cells in cochlea organoids [J]. Advance Science, 2022, 9(32): e2203557.

[38] STRZALKA W, ZIEMIENOWICZ A. Proliferating cell nuclear antigen (PCNA): A key factor in DNA replication and cell cycle regulation [J]. Annals of Botany, 2011, 107(7): 1127−1140.

[39] SUGIMOTO N, FUJITA M. Molecular mechanism for chromatin regulation during mcm loading in mammalian cells [J]. Advances in Experimental Medicine and Biology, 2017, 1042: 61−78.

[40] SUN Xiao-ming, KAUFMAN P D. Ki-67: More than a proliferation marker [J]. Chromosoma, 2018, 127(2): 175−186.

[41] OZGUR E, GÜLER G, SEYHAN N. Mobile phone radiation-induced free radical damage in the liver is inhibited by the antioxidants N-acetyl cysteine and epigallocatechin-gallate [J]. International Journal of Radiation Biology, 2010, 86(11): 935−945.

[42] WANG Ya-qi, ZHANG Yi, ZHANG Xiao-min, YANG Ting-ting, LIU Chen-geng, WANG Pei-chang. Alcohol dehydrogenase 1B suppresses β-amyloid-induced neuron apoptosis [J]. Frontiers in Aging Neuroscience, 2019, 11: 135.

[43] BERTHON J Y, NACHAT-KAPPES R, BEY M, CADORET J P, RENIMEL I, FILAIRE E. Marine algae as attractive source to skin care [J]. Free Radical Research, 2017, 51(6): 555−567.

[44] YI Ruo-kun, TAN Fang, LIAO Wei, WANG Qiang, MU Jian-fei, ZHOU Xian-rong, YANG Zhen-nai, ZHAO Xin. Isolation and identification of lactobacillus plantarum HFY05 from natural fermented yak yogurt and its effect on alcoholic liver injury in mice [J]. Microorganisms, 2019, 7(11): 530.

[45] LIN Fei, XIAO Jing-yuan, LIANG Fang-te, DAI Hui-jun, YE Liu, JING Ren, LIN Jin-yuan, PAN Ling-hui. Preconditioning with rHMGB1ameliorates lung ischemia-reperfusion injury by inhibiting alveolar macrophage

pyroptosis via the Keap1/Nrf2/HO-1 signaling pathway [J]. Journal of Translational Medicine, 2020, 18(1): 301.

[46] ZHU Yi-yun, WANG Kang, JIA Xin-yi, FU Cai-li, YU Hai-ning, WANG Yi-peng. Antioxidant peptides, the guardian of life from oxidative stress [J]. Medicinal Research Reviews, 2024, 4(11): 275−364.

[47] SHIEKH P A, SINGH A, KUMAR A. Engineering bioinspired antioxidant materials promoting cardiomyocyte functionality and maturation for tissue engineering application [J]. ACS Applied Materials & Interfaces, 2018, 10(4): 3260−3273.

[48] FRAZÃO L P, CASTRO J V D, NEVES N M. In vivo evaluation of the biocompatibility of biomaterial device [J]. Advances In Experimental Medicine and Biology, 2020, 1250: 109−124.

[49] MOHAMED Q, ZAMIR E. Update on Fuchs' uveitis syndrome [J]. Current Opinion in Ophthalmology, 2005, 16(6): 356−363.

[50] SCHITTENHELM L, HILKENS C M, MORRISON V L. β_2 integrins as regulators of dendritic cell, monocyte, and macrophage function [J]. Frontiers in Immunology, 2017, 8: 1866.

[51] KOCHUMON S, MADHOUN A A, AL-RASHED F, THOMAS R, SINDHU S, AL-OZAIRI E, AL-MULLA F, AHMAD R. Elevated adipose tissue associated IL-2expression in obesity correlates with metabolic inflammation and insulin resistance [J]. Scientific Reports, 2020, 10(1): 16364.

[52] SCHRÖDER A, NAZET U, MUSCHTER D, GRÄSSEL S, PROFF P, KIRSCHNECK C. Impact of mechanical load on the expression profile of synovial fibroblasts from patients with and without osteoarthritis [J]. International Journal of Molecular Sciences, 2019, 20(3): 585.

[53] GHASEMI H. Roles of IL-6 in ocular inflammation: A review [J]. Ocular Immunology and Inflammation, 2018, 26(1): 37−50.

[54] ZHANG Peng, YIN Yu-ping, WANG Tao, LI Wei, LI Cheng-guo, ZENG Xiang-yu, YANG Wen-chang, ZHANG Rui-zhi, TANG Yu, SHI Liang, LI Rui-dong, TAO Kai-xiong. Maresin 1 mitigates concanavalin A-induced acute liver injury in mice by inhibiting ROS-mediated activation of NF-kappaB signaling [J]. Free Radical Biology and Medicine, 2020, 147: 23−36.

[55] PADGETT L E, BURG A R, LEI Wei-qi, TSE H M. Loss of NADPH oxidase-derived superoxide skews macrophage phenotypes to delay type 1diabetes [J]. Diabetes, 2015, 64(3): 937−946.

[56] ZHANG Yan, CHOKSI S, CHEN Kun, POBEZINSKAYA Y, LINNOILA L, LIU Zheng-gang. ROS play a critical role in the differentiation of alternatively activated macrophages and the occurrence of tumor-associated macrophages [J]. Cell Research, 2013, 23(7): 898−914.

[57] SHAW T J, KISHI K, MORI R. Wound-associated skin fibrosis: mechanisms and treatments based on modulating the inflammatory response [J]. Endocrine Metabolic & Immune Disorders-Drug Targets, 2010, 10(4): 320−330.

[58] PELLICORO A, RAMACHANDRAN P, IREDALE J P, FALLOWFIELD J A. Liver fibrosis and repair: Immune regulation of wound healing in a solid organ [J]. Nature Reviews Immunology, 2014, 14(3): 181−194.

Nb_2C MXene 薄膜眼部植入体的生物相容性

马 巍[1,2]，彭 立[1,3]，陈百华[1,2]

1. 中南大学 湘雅二医院 眼科，长沙 410011；
2. 湖南省眼科临床研究中心，长沙 410011；
3. 中南大学 湘雅医学院附属海口医院 眼科，海口 570311

摘 要：采用四氟硼酸(HBF_4)与氢氟酸(HF)复合酸蚀刻和真空抽滤法制备 Nb_2C MXene 薄膜。利用扫描电子显微镜(SEM)、原子力显微镜(AFM)和 X 射线光电子能谱(XPS)等方法表征 Nb_2C MXene 的表面结构、性质和组成。通过体内和体外实验评价 Nb_2C MXene 薄膜的生物相容性。结果表明，Nb_2C MXene 具有层状、微纳表面结构，表面富集大量羟基。相比于对照组，1 mg/mL Nb_2C MXene 培养的结膜成纤维细胞增殖率达到 72.15% (p<0.05)。Nb_2C MXene 的细胞毒性评估为 0 级 (p>0.05)，其溶血率为 0.38% (<5%)。Nb_2C MXene 薄膜降低兔眼组织的炎症和氧化应激反应，在不诱导纤维化的情况下促进伤口愈合，其微纳表面促进细胞的黏附和增殖，表现出良好的生物相容性。

关键词：Nb_2C MXene；生物相容性；氧化应激；细胞增殖；眼科应用

(Edited by Bing YANG)